COMPUTATIONAL AND EXPERIMENTAL EVALUATION OF ACTUATING SHAPE MEMORY POLYMER FOAMS IN THE CONTEXT OF ANEURYSM TREATMENT

An Honors Fellows Thesis

by

EDWARD KARL HAHN III

Submitted to the Honors Programs Office
Texas A&M University
in partial fulfillment of the requirements for the designation as

HONORS UNDERGRADUATE RESEARCH FELLOW

April 2010

Major: Biomedical Engineering

COMPUTATIONAL AND EXPERIMENTAL EVALUATION OF ACTUATING SHAPE MEMORY POLYMER FOAMS IN THE CONTEXT OF ANEURYSM TREATMENT

An Honors Fellows Thesis

by

EDWARD KARL HAHN III

Submitted to the Honors Programs Office
Texas A&M University
in partial fulfillment of the requirements for the designation as

HONORS UNDERGRADUATE RESEARCH FELLOW

Approved by:

Research Advisor: Duncan J. Maitland
Associate Director of the Honors Programs Office: Dave A. Louis

April 2010

Major: Biomedical Engineering

ABSTRACT

Computational and Experimental Evaluation of Actuating Shape Memory Polymer Foams in the Context of Aneurysm Treatment. (April 2010)

Edward Karl Hahn III
Department of Biomedical Engineering
Texas A&M University

Research Advisor: Dr. Duncan J. Maitland
Department of Biomedical Engineering

Shape memory polymer foams may be used to treat vascular aneurysms through thermal actuation of the foam from a compacted to an expanded configuration within the aneurysm structure, thereby alleviating blood pressure on the weakened aneurysm walls and reducing potential for rupture. After delivery to the aneurysm site, fiber-delivered laser light absorbed by the foam structure is converted into thermal energy, and actuation of the foam results. Introduction of nonphysiological energy into the body during foam actuation necessitates an evaluation of potential thermal damage to nearby tissue.

In the present investigation, the foam is idealized as a heat-dissipating, volumetrically static object centered in a straight tube of flowing water. Velocity profiles around the heat-dissipating device are acquired experimentally with particle image velocimetry. A computational fluid dynamics package is then used to predict the experimental velocity profiles and temperature distributions by numerical solution of the Navier-Stokes and energy equations, and agreement between the computational solution and experimental

results is assessed. Discussion of this assessment, as well as several preliminary procedures leading up to the creation of the heat-dissipating device and critical analysis of the methods employed, is also given. PIV and CFD are found to be in reasonable agreement with one another. Using laser-induced fluorescence as a temperature measurement modality, which is discussed in the text insofar as the technique was attempted several times and failed, together with PIV and CFD provides a formidable array of techniques exists to characterize flow around a heated device.

DEDICATION

If the work I have performed is somehow worthy of giving to another, I freely give it to my heavenly Father Who continuously bestows upon me blessing after blessing when I am deserving of much less. Thank You, Father, for the love You have shown me in Your Son and in my short but lengthening journey through this life You have given me. To You alone be the glory.

ACKNOWLEDGMENTS

I owe a debt of gratitude to my parents for their unwavering support and encouragement, but most of all their love. I cannot ask for better. Thank you.

Thanks also to Mr. Howard Terry for graciously funding the college education of a kid from Georgetown, TX whom you had never met before. I believe your investment has not been wasted. Thank you.

I also wish to acknowledge Dr. Duncan Maitland for allowing an overambitious undergraduate to think and act like a graduate student and for freely setting before me opportunities unheard of elsewhere. Thank you.

Thanks also to the Biomedical Device Laboratory group, specifically Wonjun Hwang and Jennifer Rodriguez, for patient assistance, advice, and hours of conversation about the lab and life. Thank you.

Finally, I wish to acknowledge NIH/NIBIB Grant R01EB000462 and the Texas A&M University Honors Program for funding used to support this work.

NOMENCLATURE

CFD	Computational Fluid Dynamics
LIF	Laser-induced Fluorescence
PIV	Particle Image Velocimetry
SMP	Shape Memory Polymer

TABLE OF CONTENTS

CHAPTER Page

LIST OF FIGURES

CHAPTER I

INTRODUCTION

Motivation

In the science of medical device design there is a need for accurate computational modeling and corresponding experimental validation of device characteristics. Experimentally verified computational models provide a means of predicting device performance and failure in the body. The goal of the present work is to evaluate the agreement between two analogous experimental and computational approaches to flow velocity and temperature field characterization in the context of an academic formulation of shape memory polymer foam actuation within an aneurysm.

Particle image velocimetry (PIV) and laser-induced fluorescence (LIF) techniques are employed with the intent of quantitatively measuring the velocity and temperature fields, respectively, around an idealized shape memory polymer foam device undergoing actuation. The PIV technique elucidates flow velocities by seeding the flow field with tracer particles and imaging the tracer particles at two successive instants with a known intervening time increment. The two images are analyzed using the cross-correlation statistical technique to determine the direction of all particle displacements in the flow

---

This thesis follows the style of *IEEE Transactions on Biomedical Engineering*.

field. In a similar manner, the LIF technique seeds a flow with two fluorescent dyes, exactly one of which possesses temperature-dependent fluorescent intensity. Flow field imaging is according to the fluorescent intensities of the dyes, which are compared to a calibration standard to determine fluid temperature. Taken together, the PIV and LIF techniques empirically determine velocity and temperature fields within a flow field at discrete points.

The computational fluid dynamics (CFD) technique is the computational analogue of the PIV and LIF techniques. An experimental flow field is modeled using a computer-aided design package and discretized into volumetric elements, and the governing equations are solved iteratively to convergence for each element. Velocity and temperature information are extracted from the volumetric elements, yielding the computational analogue of the experimental PIV and LIF results and enabling quantitative comparisons between the empirical data and theoretical expectations.

Scope of thesis

An evaluation of the agreement between experimental (PIV) and computational (CFD) techniques for flow field characterization, specifically the associated velocity field, is provided in the following chapters. LIF is discussed insofar as the experimental procedure and potential improvements to gain accurate results, but reportable results were not acquired and are not presented.

Chapter II provides necessary context to the present investigation. Relevant background on aneurysm and shape memory polymers is given, and the experimental and computational techniques employed are explained in detail. Chapter II closes with a precise statement of the problem addressed in this work.

A review of the literature is given in Chapter III and is used to demonstrate the dearth of information concerning medical device characterization utilizing experimental techniques such as PIV and LIF.

Chapter IV describes the methods followed in this work. An overview of the philosophical approach taken to formulation of the problem statement into experiment is provided. The steps taken for both the experimental and computational approaches are described in detail.

Chapter V presents the experimental and computational results obtained from the methods described in Chapter IV. The chapter closes with a discussion of the results. This discussion includes detailed comparisons of the results, and analysis of the agreement between the experimentally and computationally obtained velocity and temperature fields.

Finally, a summary of the present work and the primary conclusions are given in Chapter VI.

CHAPTER II

BACKGROUND AND OBJECTIVE

Aneurysms

An aneurysm is a cardiovascular disease characterized by evolution of a weakening of the arterial wall into a balloon-like structure susceptible to rupture. The disease process associated with rupture of cerebral aneurysms is thought to be mediated by the interaction between hemodynamic forces and the arterial wall biology [1]. The rupture of intracranial aneurysms accounts for 80 percent of nontraumatic subarachnoid hemorrhage (SAH) cases. Nearly half of the survivors of SAH will be afflicted long-term cognitive impairment [2].

A number of hemodynamic characteristics have been implicated in the rupture of saccular aneurysms, including concentrated inflow jets with small impaction zones, elevated wall shear stress, and complex unstable flow patterns [3]. Indeed, unruptured aneurysms tend to exhibit hemodynamics characterized by diffuse inflow jets, large flow impingement regions, and simple stable flow patterns [4]. Because of the intimate role that hemodynamics appear to have in the rupture process of aneurysms, two current treatment methods seek to isolate the weakened wall of an aneurysm from high pressure, pulsating blood flow to prevent or treat rupture.

Current treatments

Neurosurgical clipping of the aneurysm developed first as the primary technique for treatment of SAH and involves craniotomy to access the aneurysm in question. Studies in the 1960s showed the benefits outweighed risks in circumstances of favorable location of the aneurysm within the brain, and the risk of surgery has been progressively reduced through a variety of medical advances. Few patients, however, have been capable of returning to a normal lifestyle [5].

In 1990, the Guglielmi Detachable Coil (GDC) was introduced as an alternative treatment modality for aneurysms [5-7]. GDC treatment promotes thrombus formation within the aneurysm structure. The device consists of a soft platinum coil soldered to a stainless steel delivery wire and is delivered via endovascular approach. Specifically, treatment relies on the principals of electrothrombosis and electrolysis. Electrothrombosis results from the attraction of negatively charged blood components, such as red and white blood cells, to a positively charged electrode; thrombosis is promoted by this process. Electrolysis of the solder enables intra-aneurysmal placement of the platinum coil [7]. Overall, the literature shows the GDC technique to be widely successful compared to previous techniques [5, 8, 9], but since its inception, the technique has suffered from a number of deficiencies, including incomplete aneurysm occlusion [6], instability of coiling over time [10], inability to effectively treatment large aneurysms [10, 11], and time-consuming surgery [12]. An alternative treatment modality using shape memory polymer (SMP) foam to fill aneurysms has been proposed and is

currently in development by Lawrence Livermore National Laboratory and the Biomedical Device Laboratory at Texas A&M University.

Proposed treatment

In general, SMPs form a class of so-called smart materials capable of mechanical actuation from one configuration to another in response to a stimulus [13]. In the present case, the stimulus of interest is heat. Heating raises the temperature of the SMP foam above its glass transition temperature, thereby decreasing the elastic modulus of the material and promoting foam expansion from the compressed state required for catheter delivery to the full volume of the aneurysm. Advantages to SMP foam treatment will include endovascular treatment via catheter, faster treatment time, and 60-fold expansion capabilities from the crimped state required for endovascular delivery [12]. Importantly, if the glass transition temperature of the SMP foam is above body temperature, an energy source external to the body must be used to heat the foam *in* vivo to achieve actuation and filling of the aneurysm. The introduction of non-physiologic energy into the body necessitates determination of potential thermal damage to blood and surrounding tissue. Analysis of this problem as it pertains to a heat-dissipating device in the body is the basis for the present inquiry.

Techniques

Particle image velocimetry

PIV is a technique used to indirectly measure fluid velocity fields. It relies on measurement of tracer particle positions with known time increments between the positions. Knowledge of both these parameters—particle positions and time between positions—enables calculation of particle velocity. If the properties of the tracer particles are not too different from the properties of the fluid, then the particle velocities are a good estimation of the fluid velocity [14].

In the present investigation, particle positions are acquired by 2 CCD cameras and double pulse illumination of the flow field around the heat-dissipating device being studied. Importantly, the illumination is provided in the form of a so-called light sheet, allowing for the approximation that the images acquired contain data from a plane. The double pulse illumination is provided by a Nd:YAG laser, and the pulse sequence timing corresponds to the exposure sequence of the CCD cameras. Each camera is exposed twice per set of illuminating pulses, once for each pulse, giving 2 sets of 2 images. Each image set meets the criteria described above. The two images in a set contain information regarding particle position, and the time-lapse between laser pulses determines the separation of the particles in the image.

To determine velocities in the flow field, each image in a set is divided into interrogation windows and cross-correlation between the images. The correlation technique is described by the following equation:

$$C(dx,dy) = \sum_{x=0,y=0}^{x<n,y<n} I_1(x,y)I_2(x+dx,y+dy), \quad -\frac{n}{2} < dx,dy < \frac{n}{2}, \tag{1}$$

where I_1, I_2 are image intensities of the 1st and 2nd interrogation windows, respectively; $C(dx,dy)$ is the correlation strength based on the displacements dx and dy; and n is the size of the interrogation window. This function basically determines if a pattern of particles appears shifted in the interrogation window, and if so in what direction and magnitude; the peak value in $C(dx,dy)$ is the indicator of this information. Performing cross-correlation for a series of image sets provides information on characteristics of the flow field, namely the desired velocity field [15].

Laser-induced fluorescence

LIF is an imaging technique similar used to acquire flow field temperature measurements. In the present investigation, the fluid is seeded with two fluorescent dyes: Rhodamine 110 and Rhodamine B. Rhodamine B exhibits temperature-dependent fluorescence, with intensity changes on the order of 2 percent per degree Celsius. Illuminating the flow with a Nd:YAG laser stimulates the dyes, which then fluoresce at different wavelengths. The ratio of the intensity of Rhodamine B fluorescence to

Rhodamine 110 fluorescence can be used in combination with a calibration to determine fluid temperature differences in a flow field.

Computational fluid dynamics

CFD is based on the continuum assumption: the equations that govern the whole also govern arbitrarily sized computational elements in the domain. The smaller the computational elements are, the better the resulting numerical approximation is to the actual solution of the governing equations—and presumably to reality. Three primary governing equations are of interest in the present investigation: the continuity, momentum, and energy equations. When these equations are iteratively solved to convergence for the computational elements of interest, velocity and temperature information corresponding to flow of a certain fluid at the location of the computational element may be obtained.

For the computational results to approximate reality as closely as possible, the computational domain should also closely resemble reality. This criterion may be accomplished by modeling the real experimental setup with a CAD package, then meshing the model to obtain the individual computational elements. The size and shape of the computational elements is important to the speed with which the solver is able to converge to a solution, as well as to the accuracy of the solution. Larger computational elements will not be able to adequately resolve finer details in the flow, but many

smaller elements will require significant computing time to arrive at a solution. A balance between these two conditions is necessary.

The choice of boundary conditions is also of critical importance. Replicating the dimensions of an experiment within a CAD package is relatively simple. Choosing boundary conditions that mimic real life is not as simple, and is a major challenge in obtaining accurate results. For this reason, several critical measurements are acquired from the experimental setup in the present investigation that may be inputted into the computational model, namely inlet flow rate and internal temperature of the heat-dissipating device.

Objective

The goal of the present investigation is to utilize the experimental PIV and LIF techniques in combination with CFD to attempt an analysis of fluid velocity and temperature around a heat-dissipating device in a flow. The present investigation is essentially an analysis of the applicability of the above techniques to the problem of characterizing actuating SMP foams.

CHAPTER III

LITERATURE REVIEW

Computational fluid dynamics

The literature shows significant breadth work in the field of cardiovascular fluid mechanics [16], and the use of both CFD and PIV is well-represented. A number of studies have employed CFD to aneurysm specific investigations, and the use of patient-specific computational geometries has proved useful [17]. Cebral *et al.* constructed 62 patient-specific models of cerebral aneurysms from 3D angiographic data for the purposes of CFD investigation [18, 19]. Simulated flow patterns within the aneurysms were used as a basis for categorization of the aneurysm geometries. Flow within more than 70 percent of the aneurysms that ruptured was characterized by at least one of the following phenomena: complex or unstable flow patterns, small impingement regions, and small jet sizes. More than 73 percent of the unruptured aneurysms, however, were described by simple, stable flow patterns, large impingement regions, and large jet sizes. Steinman *et al.* sought to correlate CFD-derived flow patterns to coil compaction [17]. Hassan *et al.* utilized CFD to make recommendations on aneurysm treatment for a specific patient, as well as to predict future aneurysm growth. Their prediction was confirmed with a follow-up examination 6 months later [20]. Shojima *et al*. used CFD results to contend that wall shear stress may facilitate and trigger cerebral aneurysm rupture; wall shear stress is recommended as a metric for rupture prediction [21]. Castro *et al*. applied CFD to a variety of patient-specific aneurysms and critically assessed the

usefulness of current methods of obtaining realistic geometries [22]. Ortega *et al.* analyzed post-treatment hemodynamics of a basilar aneurysm after theoretical treatment with SMP foam to determine the potential for harmful hemodynamic stresses. Simulations predicted elevated wall shear stresses that might result in remodeling of the arterial wall [23].

CFD has also been applied to endovascular devices, such as stents, in the context of aneurysms. Stuhne *et al.* applied computational methodologies to a stented saccular aneurysm geometry. Recommendations on computational mesh requirements were made and analysis of wall shear stress distribution analyzed [24]. Radaellia *et al.* also analyzed stented aneurysms, but utilized patient-specific geometries for the analysis [25].

More relevantly, CFD simulations of an idealized heated SMP foam have been performed by Ortega *et al*. The foam was modeled as a sphere at discrete points in the actuation process, within a generic basilar aneurysm geometry. Notably, worst-case simulations predicted 25 °C aneurysm wall temperature increases as a result of foam actuation. These temperature increases were consistently at the apex of the aneurysm geometry, which exhibited the greatest isolation from convective cooling [26].

Particle image velocimetry

PIV has also been employed in a number of investigations seeking to characterize aneurysmal flow patterns. Yu *et al.* employed PIV to the investigation of abdominal

aortic aneurysms. A variety of Reynolds and Womersley numbers were considered, specifically in analyzing recirculation zones within the aneurysm [27]. Tsai *et al.* considered the vascular dynamics of a saccular basilar aneurysm. A generic geometry identical to the computational geometry employed by Ortega *et al.* was used, and overall agreement between the experimental results of Tsai *et al.* and the computational results of Ortega *et al.* was observed [28].

PIV has also been applied to flow around stents. Ionita *et al.* applied PIV to investigate the effect of asymmetric stents on blood flow [29].

Laser-induced fluorescence

LIF as a temperature measurement modality is not as well-represented as CFD or PIV in the literature, but several investigations relevant to the present work were found. Hui *et al.* and Seuntiëns *et al.* both considered heated cylinders in cross-flow using molecular tagging velocimetry and LIF, respectively. Good qualitative agreement is found between both sets of results, affirming the usefulness of whole-field fluid temperature measurements using such techniques [30, 31]. Sakakibara *et al.* and Coolen *et al.* all performed whole-field temperature measurements using Rhodamine dyes and found the measurement error to be 1.7 °C and 0.1 K, respectively. It should be noted, however, that the range of temperature of the latter was only 0.7 K, whereas the former provides results for 20-60 °C [32, 33].

Techniques in combination

Several notable investigations have combined 1 or more of the above techniques. Ford *et al.* compared PIV and CFD measurements in the same aneurysm geometry for the purpose of CFD validation, an important requirement as the sophistication of CFD models increases [34]. Baranyi *et al.* combined PIV and two different CFD codes for the purposes of analyzing cross-flow around a heated cylinder. Their results show qualitative agreement with Hui *et al.* and Seuntiëns *et al* [35]. Finally, Babiker *et al.* combined PIV and CFD to predict hemodynamics in a generic basilar artery geometry similar to that of Ortega *et al.* and Tsai *et al.* Interestingly, they modeled the influences of coil-packing density on flow dynamics, insofar as the coils affected flow in the parent vessels, but not within the aneurysm [36].

CHAPTER IV

METHODS

Philosophical approach

Computationally modeling an actuating SMP foam is not a trivial task. A variety issues arise in this endeavor: the foam structure is porous and not easily modeled in a CAD package; the shape and temperature of the foam structure are changing in time; and the *in vivo* flow conditions, blood clotting physics, and vascular anatomy are complex. These issues are not easily dealt with in the beginning of a series of experimental investigations. Rather, it is instructive to future investigation to start with a simple problem—a so-called academic problem—and gradually complicate it to analyze the entire complex problem.

To start with a simple problem, assumptions must be made in the present investigation. The complex geometry of the foam and vascular are neglected in favor of a solid, nonporous, heated metal-epoxy cap and a long, straight tube with fully developed flow. Additionally, all boundary conditions are temporally static. The result of these assumptions is a relatively simple computational model and correspondingly simple experimental setup.

Experimental methods design

PDMS model creation

A mold container was machined piecewise from acrylic sheet using a CNC (Fig. 1). A 6 mm diameter stainless steel rod served as the flow channel negative. Sufficient length was allotted to allow for full development of the flow profile within the channel. A 6 mm diameter angled inlet channel negative was machined from acrylic and held at a 45° to the flow channel negative. Aluminum adhesive tape was used to secure the pieces of the mold container. PDMS (Sylgard 184, Dow Corning) was poured into the mold and cured for 45 minutes at 80 °C. While the model was warm, the container sides and channel negatives were removed.

PDMS model holder

To ensure that the PDMS model was held rigidly in front of the PIV microscope, a multi-component holder was devised (Fig. 2). The holder consisted of an ABS plastic bottom mount adapted to the PIV system optical railing, 4 acrylic vertical supports, 2 of which were later replaced by 1/8 inch threaded rods to allow for vertical adjustments; an ABS plastic top mount adapted to the top surface of the PDMS mold; and a two-part support system to hold the device centered within the flow channel that included a 3/8 inch diameter vented cap screw and rubber pad to form a seal around the device in the manner of a Tuohy-Borst adapter. All components were held in place by 8-32 cap screws and nuts.

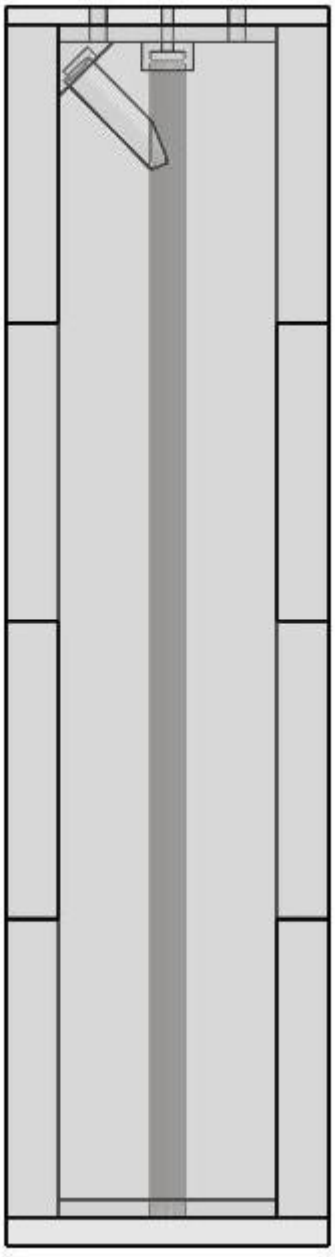

Fig. 1. PDMS model container. The container was used to cast the PDMS model used for the experimental procedures of the present investigation.

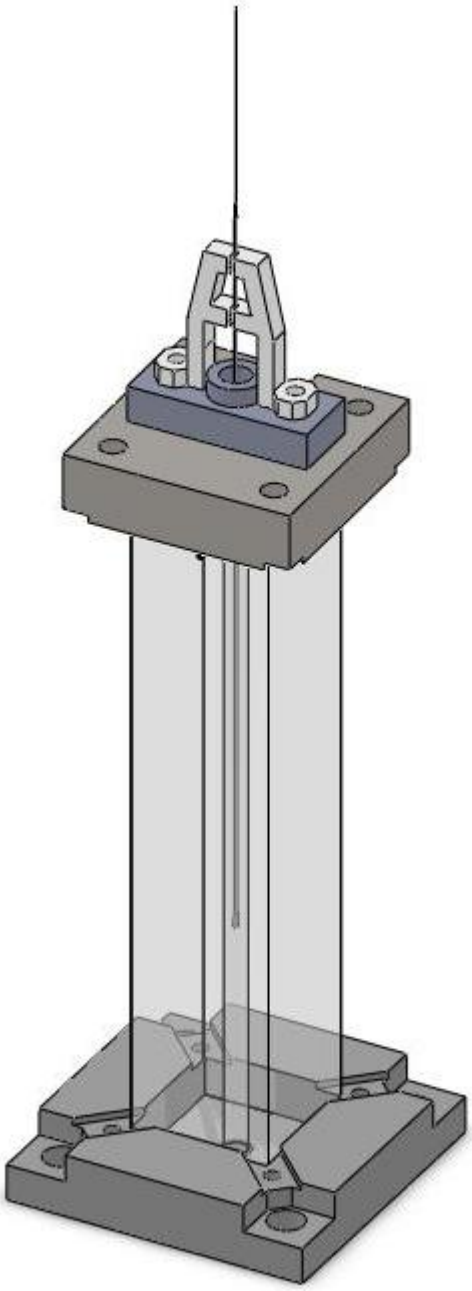

Fig. 2. Multi-component PDMS model holder. Not shown are the vertical supports. The purpose of the holder is to ensure the model remains straight and upright throughout the experiment. The device may be seen emerging from the Tuohy-Borst adapter at the top and rising well above the setup.

Flow system

A gravity-fed flow system (an elementary design of which is illustrated in Fig. 3) was constructed from 1/4 inch inner diameter Tygon tubing (VWR Scientific). An elevated reservoir was fed by a peristaltic pump drawing from a source reservoir. The elevated consisted of a funnel bound to a 1/4 inch tube adapter protruding through the bottom of a plastic beaker. An additional 1/4 inch tube adapter protruded through the bottom of the beaker and served to allow overflow to return to the source reservoir. Reservoir heights were controlled to manipulate flow rate, which was measured downstream of the device flow channel with an ultrasound flowmeter and probe (T206, Transonic Systems Inc.). To acquire downstream temperature measurements, 3 thermocouples (OMEGA) were inserted through the PDMS model and into the center of the primary flow channel 6 mm, 5 mm, and 6 mm from the position of the heat-dissipating device.

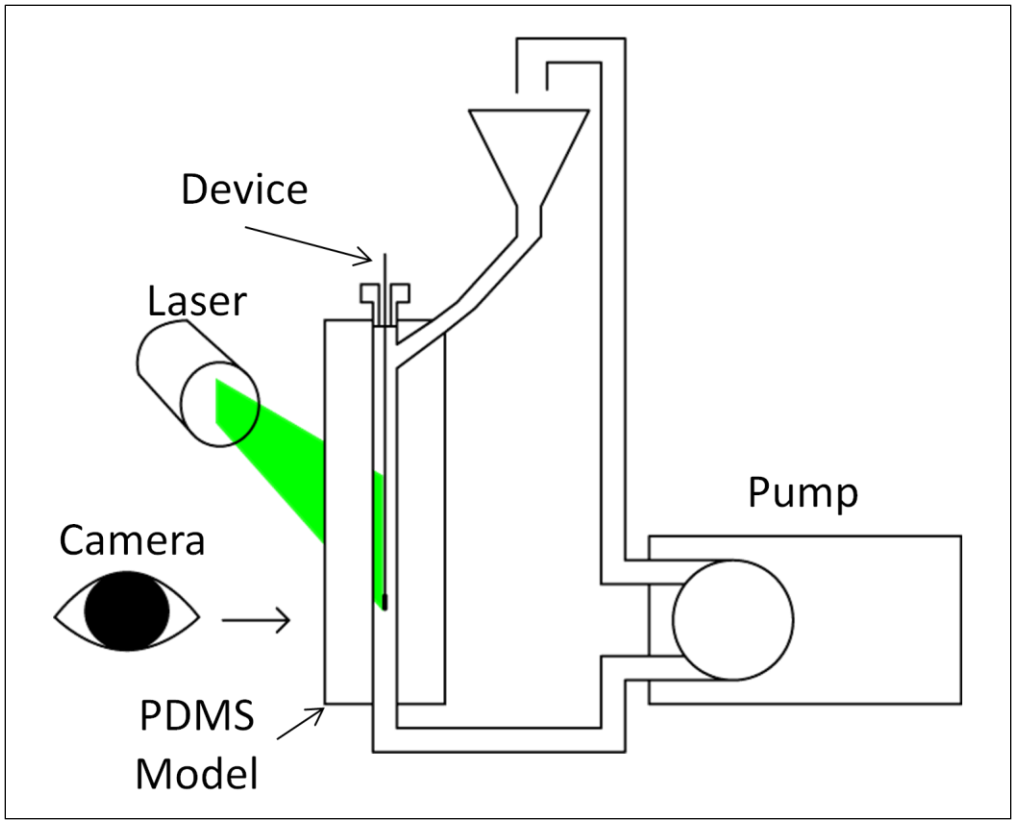

Fig. 3. Flow system. Symbolic representations of critical PIV system components are included for context. Note that the direction of the light sheet and camera view are orthogonal to one another and mutually orthogonal to the longitudinal axis of the device.

Heat-dissipating device

The heat dissipating device used to model a SMP foam in the early stages of actuation was formed from multiple components. A 200 μm optical fiber (Polymicro Industries, LLC) was terminated in a thermally conductive epoxy (H70E-2, Epo-Tek) contained within a metal cap with a 0.150 inch deep, 0.035 inch inner diameter hold machined from a 4 mm long, 0.052 inch outer diameter stainless steel 17-4 PH rod (Small Parts, Inc.). The fiber was approximately concentric with the metal cap and inserted about 0.120 inches into the thermally conductive epoxy. Additionally, the junction of a 0.003 inch T-type thermocouple (OMEGA) was terminated in the thermally conductive epoxy at the maximal depth to the side of the optical fiber. The thermally conductive epoxy was then cured for 20 minutes at 100 °C and 1 hour at 150 °C. At this point, calorimetric experiments were performed; see *Calorimetry*. The optical fiber and one thermocouple lead were bundled together in a Teflon sheath to insulate the thermocouple leads from one another. The bundle and the unsheathed thermocouple lead were drawn through a 0.042 inch outer diameter, 0.032 inch inner diameter stainless steel 304 tube (Small Parts, Inc.). This catheter-like tube served to support the heat-dissipating metal cap in the fluid flow. The metal cap and supporting tube were epoxied together with a thermally insulating epoxy (Blue-Dye Epoxy, FIS). Fig. 4 provides a graphical summary of the components of the heat-dissipating device. Fig. 5 is an image of the actual device, which is modeled in the CFD package in Fig. 6.

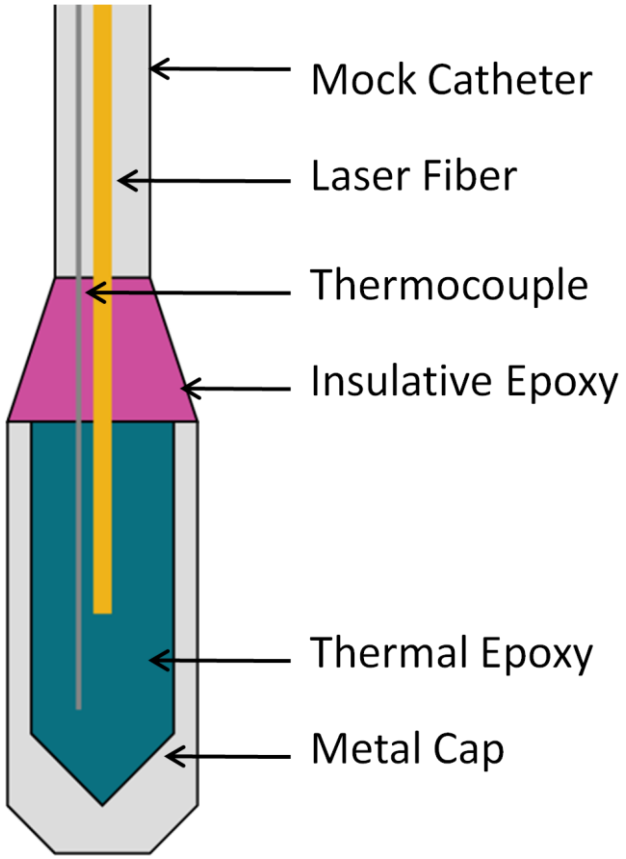

Fig. 4. Cross-sectional schematic of heat-dissipating device.

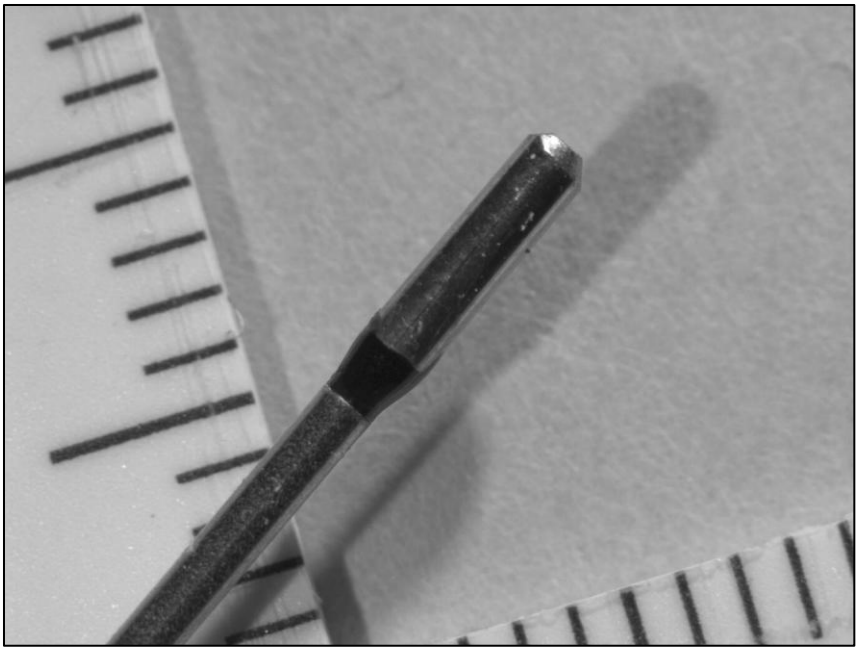

Fig. 5. Image of the actual device. The ruler scale is in millimeters.

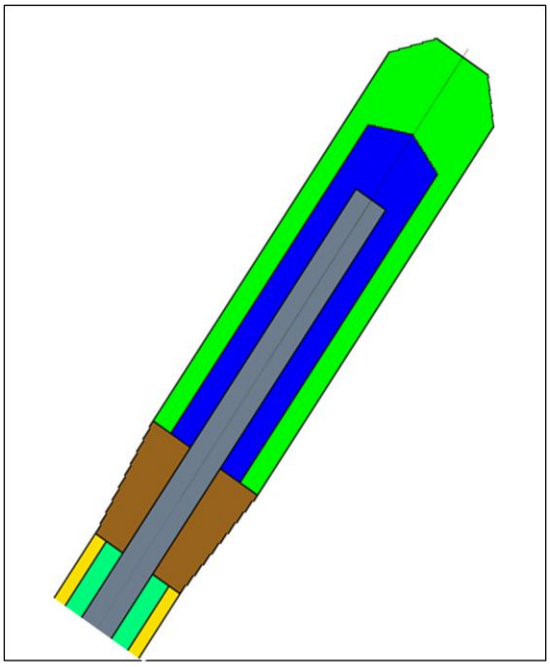

Fig. 6. Computational model of the heat-dissipating device. Colors distinguish unique material regions. Note the similarity in shape to the real device in Fig. 5.

Laser and measurement control

A master LabVIEW VI (National Instruments) and serial communication sub-VIs were developed to control both the heat source of the device and the temperature and flow measurements. The energy source for the heat-dissipating device was an 810 nm infrared laser (UM7800, Unique M.O.D.E.). Temperature and flow data were acquired with NI 9219 and NI USB-6251 DAQ devices (National Instruments), respectively.

Current-power measurements

To determine the power output of the of the UM7800 laser, a power meter (PM300E, Thorlabs) and thermopile (S212A, Thorlabs) were used. Power readings were acquired with currents ranging from 1 A to 5.5 A; steady-state power readings were recorded. Linear regression was performed on the resulting data set to acquire power as a function current.

Calorimetry

A calorimeter was constructed from a 2 foot cube of extruded polystyrene (EPS) (Texas Foam). The cube was cut in half using resistively heated steel music wire. Identical volumes of EPS were removed from the center of both halves to hold a 1.8 mL Nalgene cryogenic vial (VWR Scientific) of deionized (DI) water. The heat-dissipating device was inserted into the vial and the cube halves taped together.

The purpose of calorimetry is to measure energy changes associated with some process. In the present case, it is desirable to know the energy output of the heat-

dissipating device as a function of current. This output value will necessarily differ from the product of the laser power (watts) and pulse duration (seconds) because of energy losses in the fiber and thermally conductive epoxy. By measuring this property of the heat-dissipating device, efficiency of the device may be determined, which will be useful in future investigations that seek to compare the efficiencies with which particular SMP foam formulations converts laser radiation to thermal energy. The relevant equation is the specific heat formula,

$$q = mc\Delta T, \tag{2}$$

where q is the energy dissipated into the calorimeter, m is the mass of the DI water in the calorimeter container, c is the specific heat capacity of water, and ΔT is the temperature rise associated with the energy deposited by the laser pulse. Thus, for a range of laser currents, temperature rises were measured in a small mass of water insulated by the calorimeter, and the energy input was calculated using (2).

After the calorimetry experiments, the power output of the UM7800 was again measured with the power meter and thermopile, but rather than steady-state values, the time-dependent output of the laser was acquired for a set period of time. Numerically integrating this power vs. time curve using the trapezoidal rule, the actual energy output of the laser into the calorimeter is determined. Current values were chosen based on the current-power relationship determined previously, and both current values and time of laser activation were controlled by a high-speed version of the master VI detailed above to ensure laser pulse duration could be timed accurately for the calorimetry experiments.

PIV/LIF measurements

The working fluid for the present investigation was a mixture of 40% water and 60% glycerine. This mixture produces a fluid with refractive index close to that of the PDMS model at room temperature [28]. By working with a fluid of refractive index similar to the PDMS, distortions due to index changes are minimize, providing increased accuracy of measurements. PIV seeding was performed by progressively adding tracer particles to the fluid. Cameras were set to double-frame mode. Velocity measurements were initially obtained for high flow (445 mL/min) with laser currents ranging from 1.5 A to 4 A. Measurements were repeated at a lower flow rate of 100 mL/min for 0 A, 1.5 A, 2 A, and 3 A.

LIF measurements were attempted at 0 mL/min, 25 mL/min, and 50 mL/min for currents ranging from 1.5 A to 3 A.

Computational methods

CAD model

The heat-dissipating device was modeled in SolidWorks 2009 (Dassault Systemes). All unique materials composing the device were modeled as distinct volumes with the exception of the thermocouple, which was neglected. This decision was made to reduce computational complexity and exploit the axisymmetric nature of the device, support tube, and surrounding flow by only modeling sector of the experimental setup

corresponding to 22.5°. Additionally, the full length of the flow channel was modeled to allow for flow profile development within the simulation.

Meshing and boundary conditions

The CAD model was imported into Star-CCM+ 4.02.11 (CD-Adapco). Each material region was discretized and a conformal mesh generated. A base size of 0.2 mm was used as the default size, and in a cylindrical volume around the device this value was decreased to 0.04 mm to provide increased resolution of temperature and velocity gradients. There were 490846 computational elements or "cells" in the entire domain of interest.

Symmetry boundary conditions were applied appropriately. The inlet inflow velocity was specified to be the average velocity V of a flowrate Q given through a cross-sectional area A, given by equation (3).

$$V = \frac{Q}{A} \tag{3}$$

Additionally, the interface between the thermally conductive epoxy and the stainless steel cap was prescribed to be at a temperature obtained from the thermocouple embedded in the heat-dissipating device in the actual experiment.

CHAPTER V

RESULTS AND DISCUSSION

Power versus current

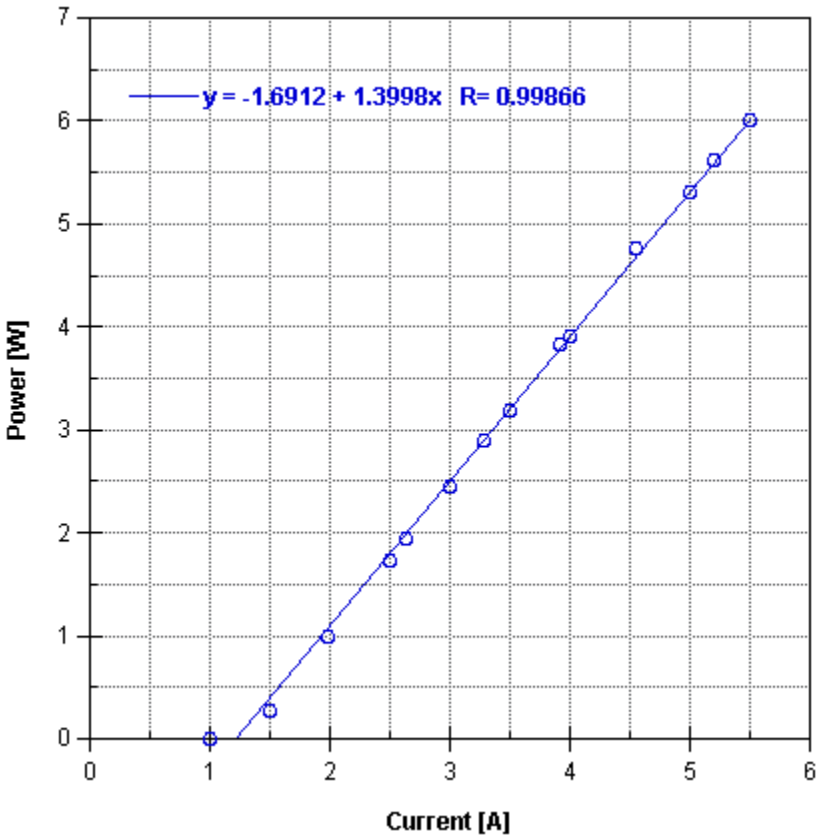

Fig. 7. Power versus current relationship for UM7800.

The power versus current curve is an important characteristic of any given laser, as it indicates the power output of the device as a function of the only parameter directly

controlled (the current). In the present case, a strong linear relationship exists between these two parameters, as evidenced by the results given in Fig. 7. This knowledge is useful in determining calorimetric data, as in the present case. It should be noted that the power values are steady-state values, obtained after a brief duration of time-dependent change in the laser output. This fact must be taken into consideration during calorimetry and any other procedure where the time-dependent energy output of the laser is of importance.

Calorimetry

Accurate calorimetry results were unable to be obtained. Surprisingly, over three independent trials, the energy input into the calorimeter water, calculated by (2), often exceeded the energy output acquired through numerical integration of the laser power output over time, and once exceeded the theoretical maximum energy input achievable. This latter case may be explained by not allowing enough time for equilibration of the calorimeter water, but in general, water temperature as measured from the (non) heat-dissipating device remained constant within measurement error for a period of several seconds before the next laser current was applied. Given the small volume of water used (less than 2 mL), such temperature consistency likely indicates that nearly uniform heat diffusion into the calorimeter water had been achieved. The former case, however, is not so easily explained.

The foam block was held together well, ruling out convective processes. Since room temperature was several degrees below calorimeter water temperature, and no heated material other than the heat-dissipating device (when the laser was activated) came into contact with the water during each experimental trial, artificial increases in water temperature may be ruled out. In fact, any contribution from the ambient environment would likely have served to decrease the measured energy input to the water. Additionally, consistency of the VI used for the calorimetry experiments had been previously verified to have consistent laser control capabilities.

One possible explanation does present itself. The time-dependent output signal of the laser was measured *after* the calorimetry experiments. After these measurements were completed, a catastrophic bend in the protective tubing housing the laser fiber was observed. The fiber had snapped. If somehow the fiber had been partially compromised during the time-dependent power measurements, it is possible that lower energy values were measured than otherwise would have been the case. This would explain the consistently high calculated energy input to the calorimeter water compared to the measured energy output of the laser integrated over time.

While efficiency may not be calculated, a benchmark to the device does exist. Proof of concept tests using a fiber terminated in a small volume of cured epoxy were measured for temperature increases when laser light was passed through the fiber. Less than 1 W of power was able to achieve temperatures of 250 °C in air. The conclusion arrived at

from these experiments is that the thermally conductive epoxy was efficient at conversion of laser light into thermal energy. The same qualitative conclusion may be applied to the heat-dissipating device.

PIV and CFD

PIV results (Figs. 8-10) are provided for 0 A, 2 A, and 3 A currents in 100 mL/min flow. The scale for the images gives velocity values mapped to colors for velocities in the range of 0-12 cm/s. Average measured temperature rises within the device were 49.6 °C and 77.0 °C for 2 A and 3 A currents, respectively. Interesting observations include the observed decrease in the thickness of the velocity boundary around the device (dark region in upper left) as current increases. Such behavior is expected: an increase in local temperature will cause a decrease in local viscosity. Boundary layer effects are dependent upon the value of the fluid viscosity, and as the fluid becomes less viscous, boundary layer effects decrease.

The correlation techniques of PIV do not always yield perfect results, as indicated by spurious vectors in the region of the device in Figs. 8 and 10. The presence of these vectors indicates the need for a stronger removal of vectors who directions do not match the directions of the surrounding flow. The physical cause of these vectors is likely movement of the device, which over a series of images might be interpreted as fluid movement during correlation.

The CFD results (Figs. 11-13) do not show the reduction in boundary layer effects associated with device heating. This suggests that the choice of material models for the water-glycerine mixture may be flawed in some way. It is also possible that surface effects of the device on the nearby fluid induced greater mixing. Specifically, the surface of the heat-dissipating device was not completely smooth as it is in the CFD simulations. Surface irregularities can promote mixing within the boundary layer, which would result in increased temperature and reduction in fluid viscosity, as observed in the PIV results.

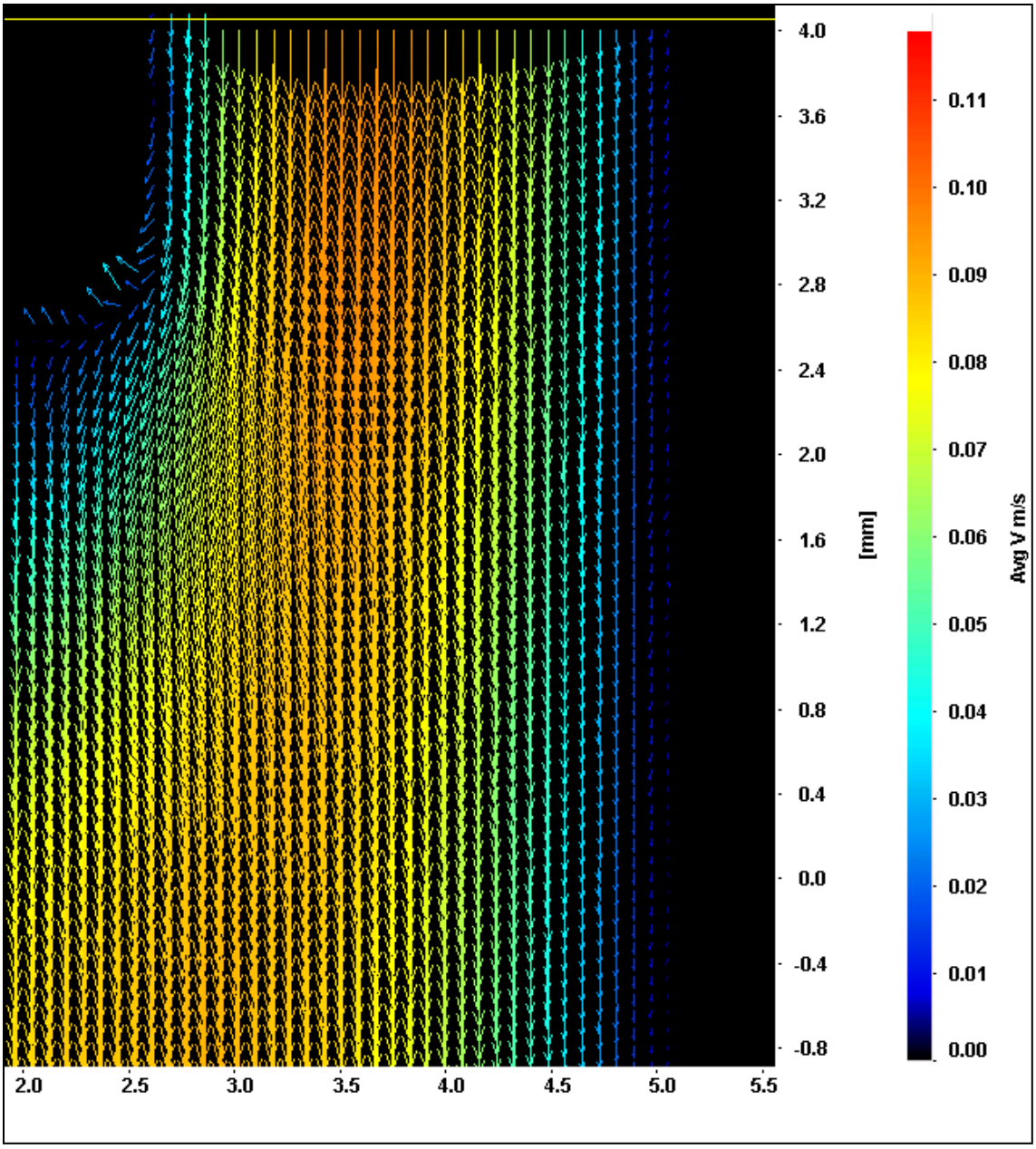

Fig. 8. PIV results for 0 A current, 100 mL/min flow.

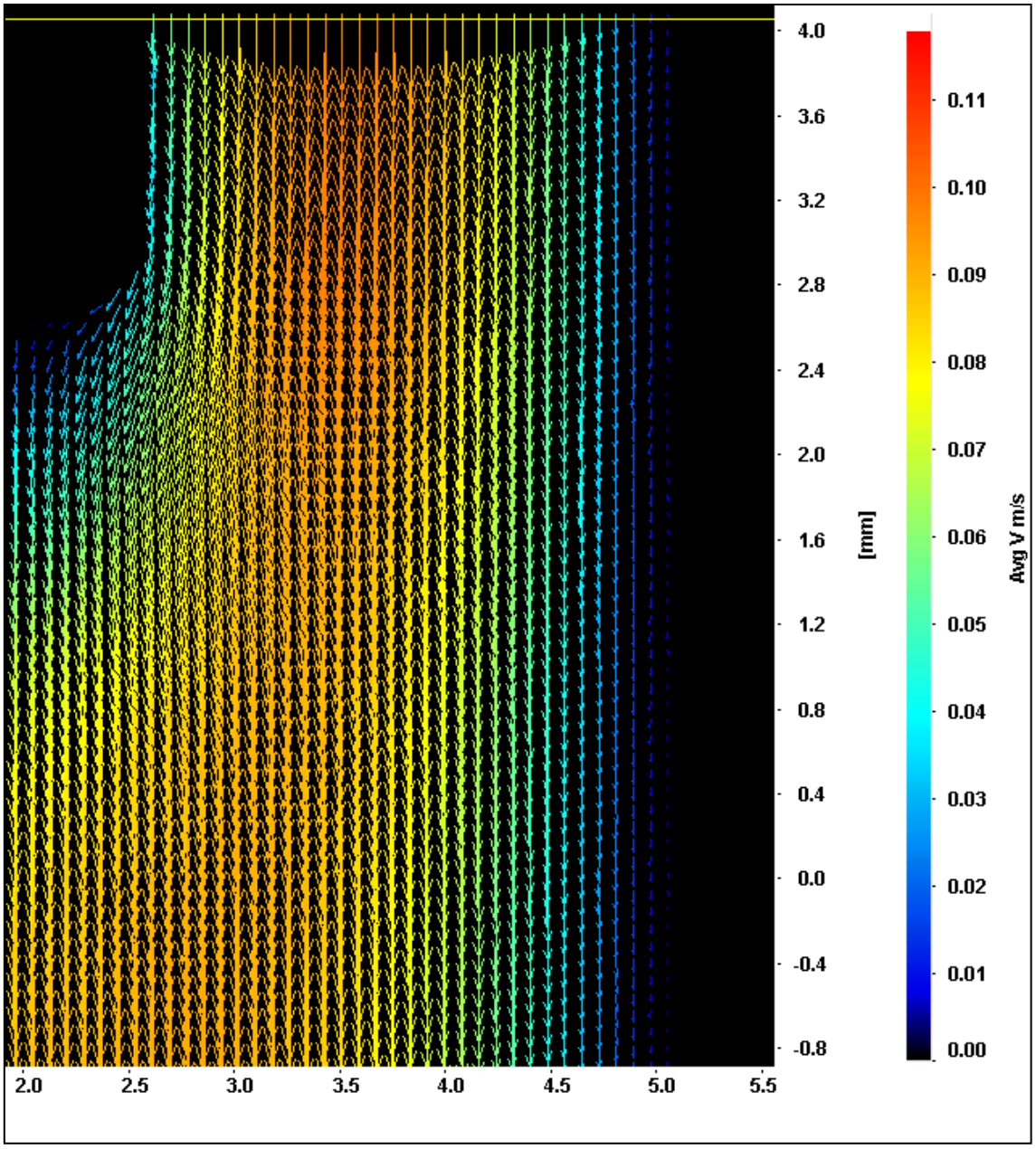

Fig. 9. PIV results for 2 A current, 100 mL/min flow.

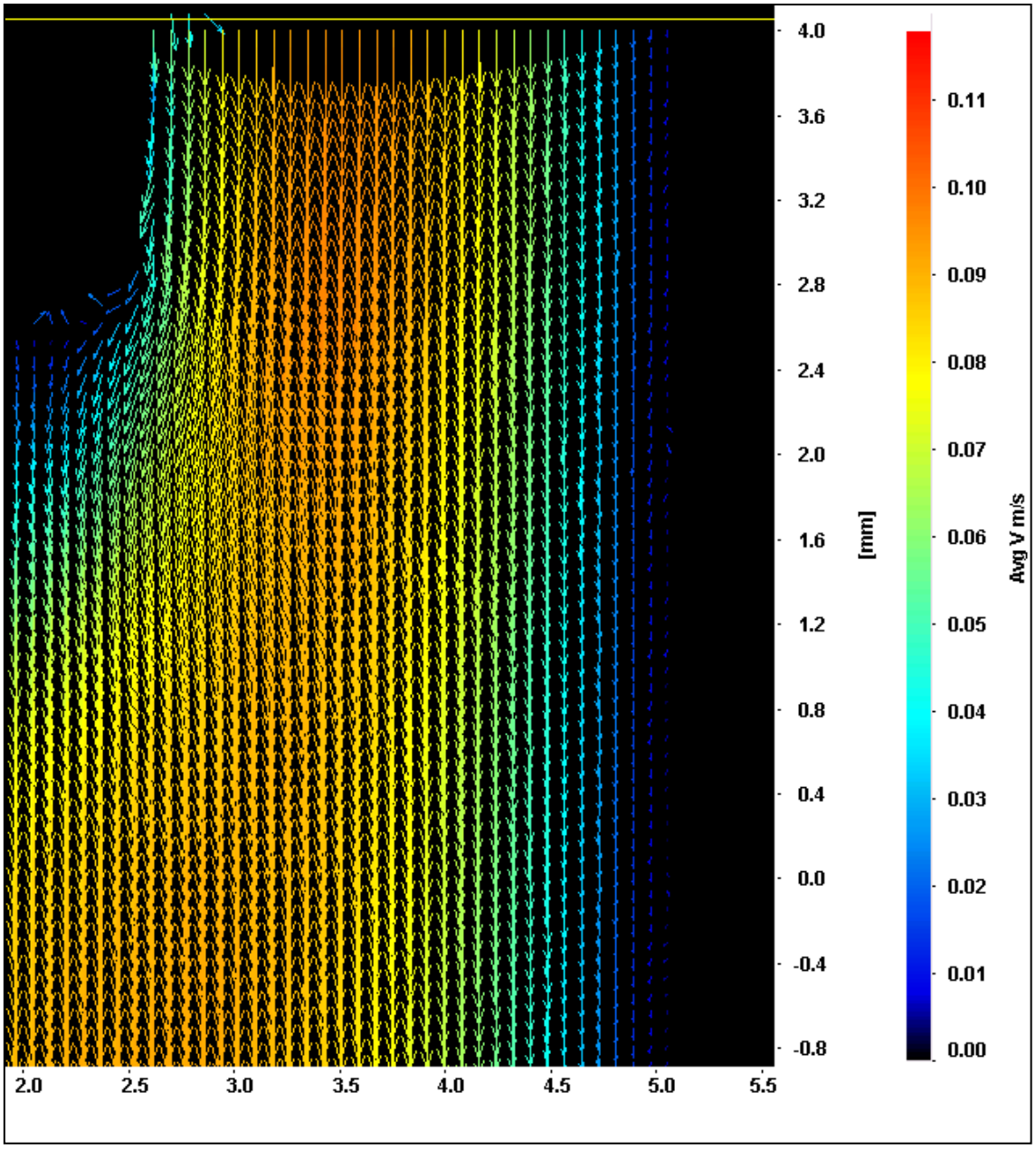

Fig. 10. PIV results for 3 A current, 100 mL/min flow.

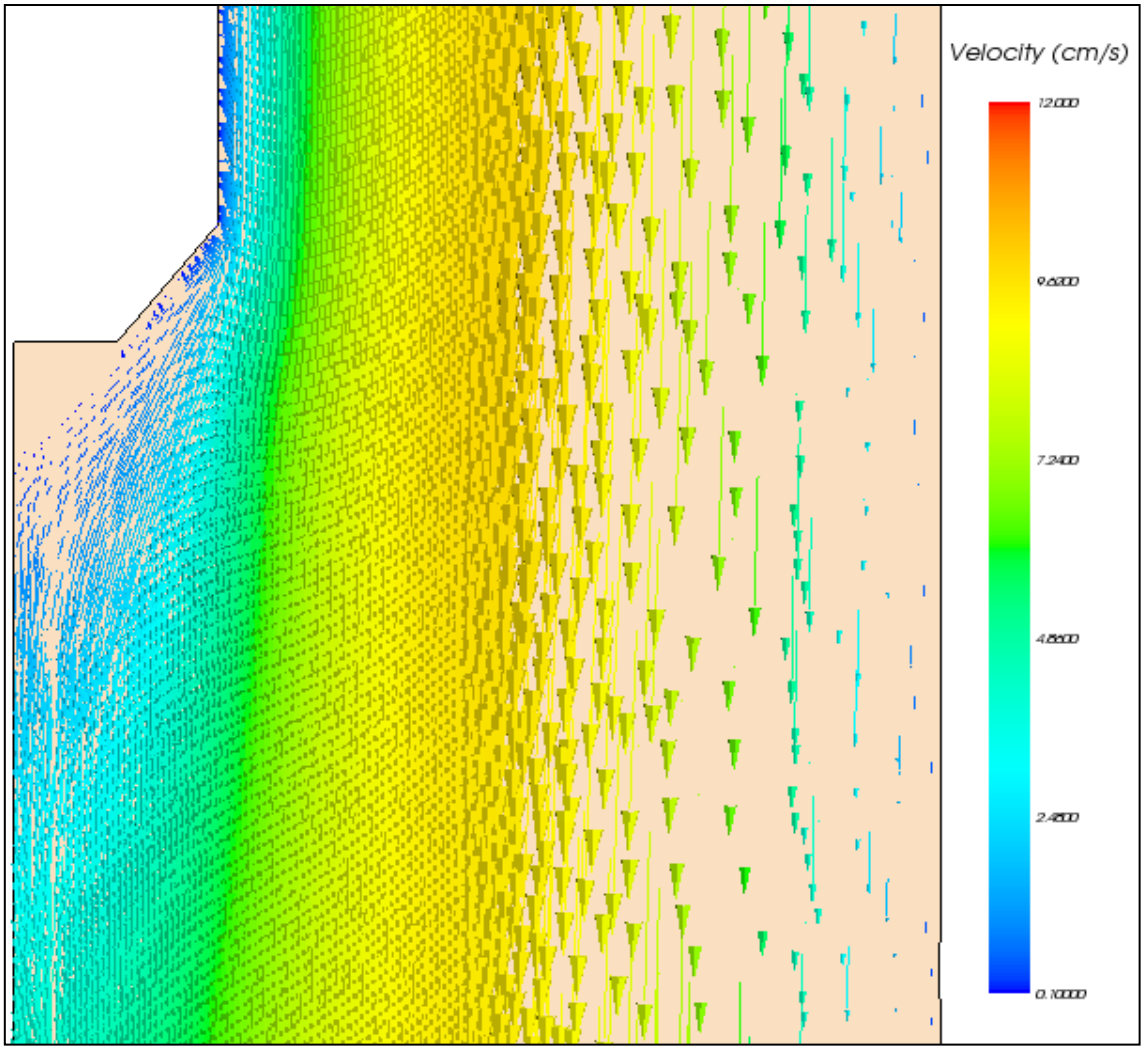

Fig. 11. CFD results for 0 A current, 100 mL/min flow.

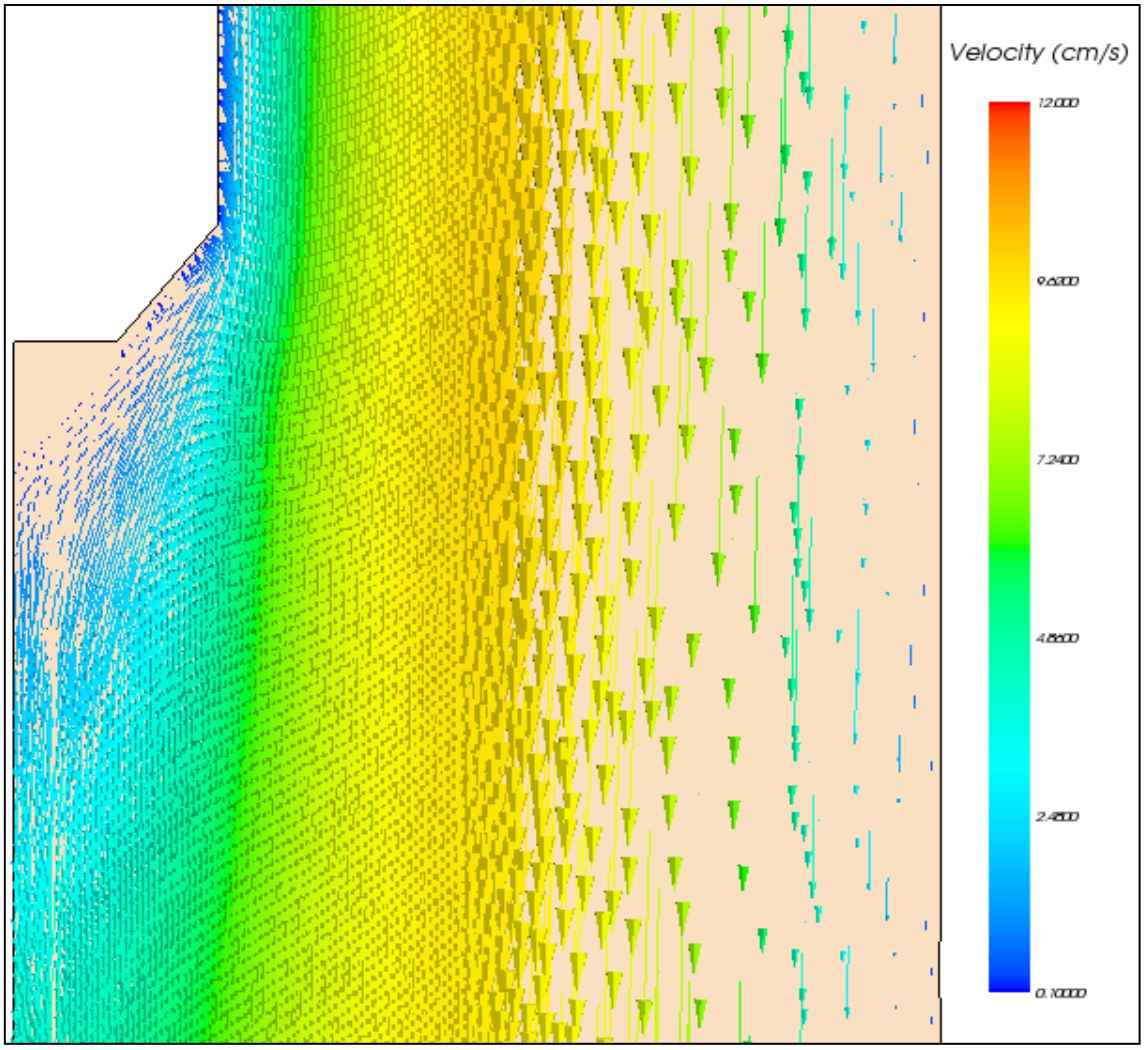

Fig. 12. CFD results for 2 A current, 100 mL/min flow.

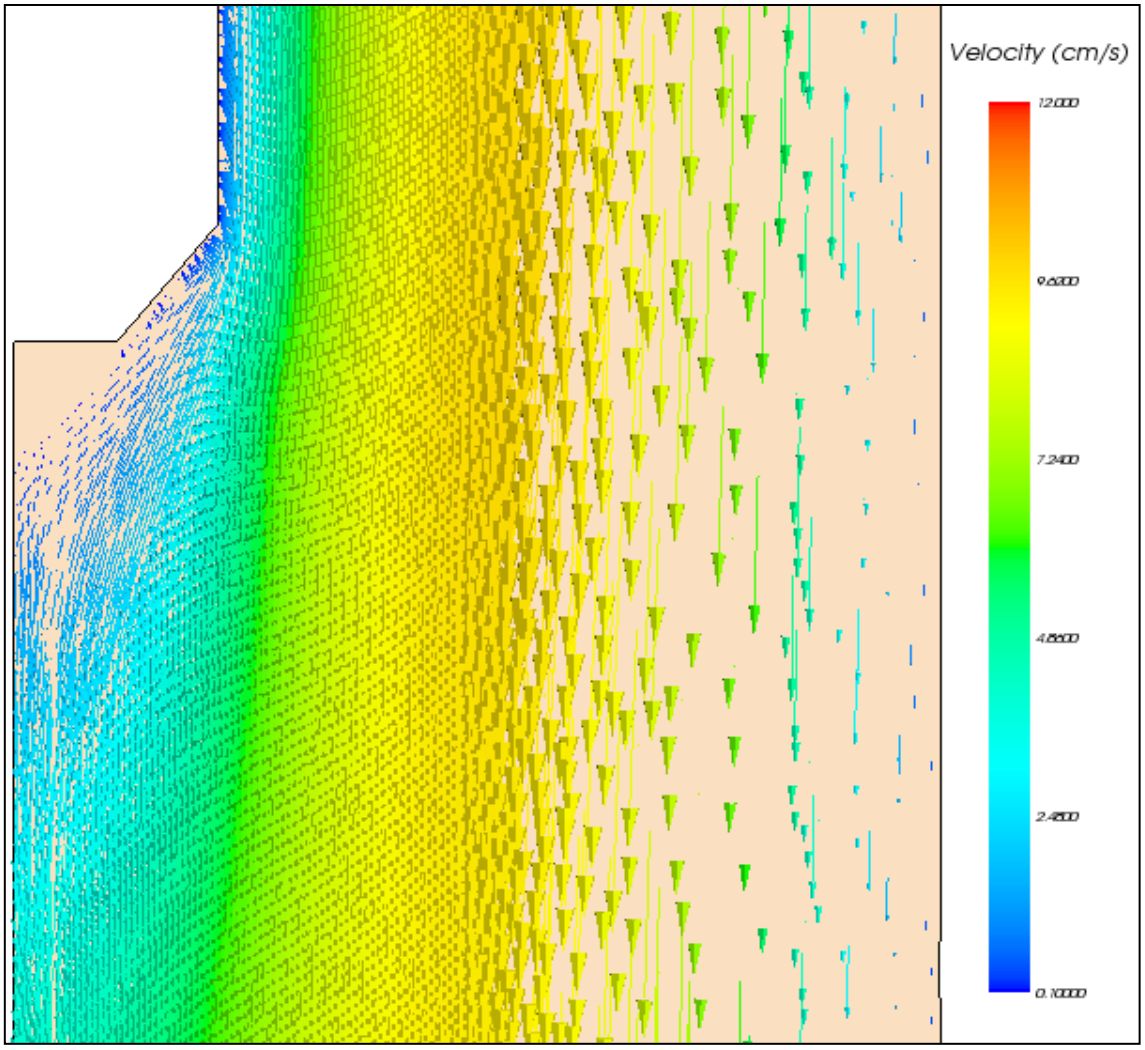

Fig. 13. CFD results for 3 A current, 100 mL/min flow.

LIF

Temperature measurements based on LIF suffered from a number of setbacks devastating to the integrity of the results. First, a reasonable level of experience using the LIF technique had not been achieved prior to measurement attempts of real data. This inexperience, in retrospect, likely affected the homogeneity with which the flow field was illuminated by the light sheet. Specifically, dye concentrations were not well managed, possibly resulting in significant intensity changes as a function of path length, a phenomenon best avoided in LIF temperature measurements.

Additionally, the heat-dissipating device suffered a minor structural failure. During laser activation, significant quantities of bubbles due to the fluid being heated obscured the device from the view of the flow field and reflected laser pulses randomly, resulting in significant illumination inhomogeneity. These bubbles had not been observed under zero flow conditions previously.

Overall, the idea of the LIF technique is promising. While intensity changes due to temperature differences were observed, difficulties in calibration made calculation of these temperature fields impossible. Combined with the failure of the device, the LIF technique was not successful in the present investigation. Success in future investigations as experience and device integrity are increased is anticipated.

CHAPTER VI

SUMMARY AND CONCLUSIONS

A complex problem with significant clinical application was reduced to an academic problem for purposes of better understanding the physical phenomena underlying the more complex problem. PIV and CFD were effectively used to characterize fluid velocities around a heat-dissipating device. LIF, while attempted, was largely unsuccessful due to inexperience and device failure. Calorimetric measurements were also unsuccessful, possibly due to a compromised laser fiber and resultant light loss.

The literature affirms the efficacy of PIV and CFD as powerful tools for experimental and computationally characterizing a flow. LIF is less well-documented, but has seen several successful implementations in the measurement of temperature fields around heat-dissipating devices. On the whole, this trio of visualization techniques has the capability to address engineering and clinical concerns in the actuation of SMP foams.

Future work in this area should include validation of LIF procedure and results with real-world measurements, followed by assessment of agreement with computational results. These tests should be performed in the same experimental/computational conditions described in the present investigation. Once the techniques have been validated in this simple case, progressively more complicated conditions should be explored, including life-like geometries of aneurysms, pulsating flow, and a porous heat-dissipating device.

Importantly, the qualitative comparisons of the present work should be extended by defining useful quantitative criteria and methodologies for evaluation, with the end goal of providing quantitative assessment of risks associated with actuation of a SMP foam device within an aneurysm.

REFERENCES

[1] M. Castro, C. Putman, A. Radaelli, A. Frangi, and J. Cebral, "Hemodynamics and rupture of terminal cerebral aneurysms," *Academic Radiology,* vol. 16, no. 10, pp. 1201-1207, 2009.

[2] J. I. Suarez, R. W. Tarr, and W. R. Selman, "Aneurysmal subarachnoid hemorrhage," *The New England Journal of Medicine,* vol. 354, no. 4, pp. 387-396, 2006.

[3] D. M. Sforza, C. M. Putman, E. Scrivano, P. Lylyk, and J. R. Cebral, "Blood-flow characteristics in a terminal basilar tip aneurysm prior to its fatal rupture," *AJNR Am J Neuroradiol*, February, 2010.

[4] J. R. Cebral, S. Hendrickson, and C. M. Putman, "Hemodynamics in a lethal basilar artery aneurysm just before its rupture," *AJNR Am J Neuroradiol,* vol. 30, no. 1, pp. 95-98, January, 2009.

[5] A. Molyneux, R. Kerr, I. Stratton, P. Sandercock, M. Clarke *et al.*, "International subarachnoid aneurysm trial (ISAT) of neurosurgical clipping versus endovascular coiling in 2143 patients with ruptured intracranial aneurysms: A randomised trial," *Lancet,* vol. 360, no. 9342, pp. 1267-1274, Oct, 2002.

[6] G. Guglielmi, F. Vinuela, J. Dion, and G. Duckwiler, "Electrothrombosis of saccular aneurysms via endovascular approach. Part 2: Preliminary clinical experience," *J Neurosurg,* vol. 75, no. 1, pp. 8-14, Jul, 1991.

[7] G. Guglielmi, F. Vinuela, I. Sepetka, and V. Macellari, "Electrothrombosis of saccular aneurysms via endovascular approach. Part 1: Electrochemical basis, technique, and experimental results," *J Neurosurg,* vol. 75, no. 1, pp. 1-7, Jul, 1991.

[8] Z. Dovey, M. Misra, J. Thornton, F. T. Charbel, G. M. Debrun *et al.*, "Guglielmi detachable coiling for intracranial aneurysms: The story so far," *Arch Neurol,* vol. 58, no. 4, pp. 559-64, Apr, 2001.

[9] A. J. Molyneux, R. S. C. Kerr, L. M. Yu, M. Clarke, M. Sneade *et al.*, "International subarachnoid aneurysm trial (ISAT) of neurosurgical clipping versus endovascular coiling in 2143 patients with ruptured intracranial aneurysms: A randomised comparison of effects on survival, dependency, seizures, rebleeding, subgroups, and aneurysm occlusion," *Lancet,* vol. 366, no. 9488, pp. 809-817, Sep, 2005.

[10] M. Sluzewski, T. Menovsky, W. J. van Rooij, and D. Wijnalda, "Coiling of very large or giant cerebral aneurysms: Long-term clinical and serial angiographic results," *AJNR Am J Neuroradiol,* vol. 24, no. 2, pp. 257-262, February, 2003.

[11] L. A. Lanterna, G. Tredici, B. D. Dimitrov, and F. Biroli, "Treatment of unruptured cerebral aneurysms by embolization with guglielmi detachable coils: Case-fatality, morbidity, and effectiveness in preventing bleeding-a systematic review of the literature," *Neurosurgery,* vol. 55, no. 4, pp. 767-775, Oct, 2004.

[12] D. J. Maitland, W. Small IV, J. M. Ortega, P. R. Buckley, J. Rodriguez *et al.*, "Prototype laser-activated shape memory polymer foam device for embolic treatment of aneurysms," *Journal of Biomedical Optics,* vol. 12, no. 3, pp. 030504 (3 pages), 2007.

[13] P. T. Mather, X. Luo, and I. A. Rousseau, "Shape memory polymer research," *Annual Review of Materials Research,* vol. 39, no. 1, pp. 445-471, 2009.

[14] M. Raffel, C. Willert, S. Wereley, and J. Kompenhans, *Particle image velocimetry, a practical guide*, 2nd ed., Berlin: Springer, 2007.

[15] "Product manual: Flowmaster," LaVision GmbH, December, 2007. Accessed at: http://www.lavision.de

[16] C. A. Taylor, and M. T. Draney, "Experimental and computational methods in cardiovascular fluid mechanics," *Annual Review of Fluid Mechanics,* vol. 36, pp. 197-231, 2004.

[17] D. A. Steinman, J. S. Milner, C. J. Norley, S. P. Lownie, and D. W. Holdsworth, "Image-based computational simulation of flow dynamics in a giant intracranial aneurysm," *American Journal of Neuroradiology,* vol. 24, no. 4, pp. 559-566, Apr, 2003.

[18] J. R. Cebral, M. A. Castro, J. E. Burgess, R. S. Pergolizzi, M. J. Sheridan *et al.*, "Characterization of cerebral aneurysms for assessing risk of rupture by using patient-specific computational hemodynamics models," *American Journal of Neuroradiology,* vol. 26, no. 10, pp. 2550-2559, Nov-Dec, 2005.

[19] J. R. Cebral, M. A. Castro, D. Millan, A. Frangi, and C. Putman, "Pilot clinical study of aneurysm rupture using image-based computational fluid dynamics models," *Medical imaging 2005: Physiology, function, and structure from medical images, pts 1 and 2*, Proceedings of the society of photo-optical instrumentation engineers (spie) A. A. Amini and A. Manduca, eds., pp. 245-256, 2005.

[20] T. Hassan, M. Ezura, E. V. Timofeev, T. Tominaga, T. Saito *et al.*, "Computational simulation of therapeutic parent artery occlusion to treat giant

vertebrobasilar aneurysm," *American Journal of Neuroradiology,* vol. 25, no. 1, pp. 63-68, Jan, 2004.

[21] M. Shojima, M. Oshima, K. Takagi, R. Torii, M. Hayakawa *et al.*, "Magnitude and role of wall shear stress on cerebral aneurysm - computational fluid dynamic study of 20 middle cerebral artery aneurysms," *Stroke,* vol. 35, no. 11, pp. 2500-2505, Nov, 2004.

[22] M. A. Castro, C. M. Putman, and J. R. Cebral, "Patient-specific computational modeling of cerebral aneurysms with multiple avenues of flow from 3D rotational angiography images," *Academic Radiology,* vol. 13, no. 7, pp. 811-821, Jul, 2006.

[23] J. Ortega, J. Hartman, J. Rodriguez, and D. Maitland, "Post-treatment hemodynamics of a basilar aneurysm and bifurcation," *Annals of Biomedical Engineering,* vol. 36, no. 9, pp. 1531-1546, 2008.

[24] G. R. Stuhne, and D. A. Steinman, "Finite-element modeling of the hemodynamics of stented aneurysms," *Journal of Biomechanical Engineering-Transactions of the ASME,* vol. 126, no. 3, pp. 382-387, Jun, 2004.

[25] A. G. Radaellia, L. Augsburger, J. R. Cebral, M. Ohta, D. A. Rufenacht *et al.*, "Reproducibility of haemodynamical simulations in a subject-specific stented aneurysm model - a report on the virtual intracranial stenting challenge 2007," *Journal of Biomechanics,* vol. 41, no. 10, pp. 2069-2081, Jul, 2008.

[26] J. Ortega, D. Maitland, T. Wilson, W. Tsai, Ö. Savaş *et al.*, "Vascular dynamics of a shape memory polymer foam aneurysm treatment technique," *Annals of Biomedical Engineering,* vol. 35, no. 11, pp. 1870-1884, 2007.

[27] S. C. M. Yu, "Steady and pulsatile flow studies in abdominal aortic aneurysm models using particle image velocimetry," *International Journal of Heat and Fluid Flow,* vol. 21, no. 1, pp. 74-83, 2000.

[28] W. Tsai, O. Savas, D. Maitland, J. Ortega, W. Small *et al.*, "Experimental study of the vascular dynamics of a saccular basilar aneurysm," *Proceedings of 2006 ASME International Mechanical Engineering Congress and Exposition*, vol. 262, pp. 317-326, November, 2006, 2006.

[29] C. N. Ionita, Y. Hoi, H. Meng, and S. Rudin, "Particle image velocimetry (PIV) evaluation of flow modification in aneurysm phantoms using asymmetric stents," vol. 5369, pp. 295-306, Feburary, 2004.

[30] H. Hui, and M. K. Manoochehr, "Molecular tagging velocimetry and thermometry and its application to the wake of a heated circular cylinder," *Measurement Science and Technology,* vol. 17, no. 6, pp. 1269, 2006.

[31] H. J. Seuntiëns, R. N. Kieft, C. C. M. Rindt, and A. A. van Steenhoven, "2D temperature measurements in the wake of a heated cylinder using LIF," *Experiments in Fluids,* vol. 31, no. 5, pp. 588-595, 2001.

[32] J. Sakakibara, and R. J. Adrian, "Whole field measurement of temperature in water using two-color laser induced fluorescence," *Experiments in Fluids,* vol. 26, no. 1, pp. 7-15, 1999.

[33] M. C. J. Coolen, R. N. Kieft, C. C. M. Rindt, and A. A. van Steenhoven, "Application of 2-d LIF temperature measurements in water using a Nd:YAG laser," *Experiments in Fluids,* vol. 27, no. 5, pp. 420-426, 1999.

[34] M. D. Ford, H. N. Nikolov, J. S. Milner, S. P. Lownie, E. M. DeMont *et al.*, "PIV-measured versus CFD-predicted flow dynamics in anatomically realistic cerebral aneurysm models," *Journal of Biomechanical Engineering,* vol. 130, no. 2, pp. 012125-1 (9 pages), 2008.

[35] L. Baranyi, S. Szabó, B. Bolló, and R. Bordás, "Analysis of low Reynolds number flow around a heated circular cylinder," *Journal of Mechanical Science and Technology,* vol. 23, no. 7, pp. 1829-1834, 2009.

[36] M. Babiker, L. Gonzalez, F. Albuquerque, D. Collins, A. Elvikis *et al.*, "Quantitative effects of coil packing density on cerebral aneurysm fluid dynamics: An in vitro steady flow study," *Annals of Biomedical Engineering*, 2010.

CONTACT INFORMATION

Name:	Edward Karl Hahn III
Professional Address:	c/o Dr. Duncan J. Maitland Department of Biomedical Engineering 337 Zachry Engineering Center Texas A&M University College Station, TX 77843
Email Address:	ekhahniii@gmail.com
Education:	B.S., Biomedical Engineering, Texas A&M University, May 2010